Research Square

Preprints are preliminary reports that have not undergone peer review.
They should not be considered conclusive, used to inform clinical practice,
or referenced by the media as validated information.

Cytotoxic and antibacterial diketopiperazine cyclic dipeptides from Streptomyces canescens associated with marine sponge Haliclona caerulea

Somayeh Zare
Bushehr University of Medical Sciences
Mohsen Gozari
Agricultural Research, Education and Extension Organization
Maryam Alborz
Shiraz University of Medical Sciences
Omidreza Firuzi
Shiraz University of Medical Sciences
Alireza Poustforoosh
Shiraz University of Medical Sciences
Hesham R. El Seedi
Jiangsu University
Amir Reza Jassbi
jassbiar@sums.ac.ir

Shiraz University of Medical Sciences

Research Article

Keywords: Haliclona caerulea, Streptomyces canescens, marine sponge-associated bacteria, symbiotic bacteria, diketopiperazine, cyclic dipeptides, DHFR, β-tubulin

Posted Date: August 25th, 2026

DOI: https://doi.org/10.21203/rs.3.rs-10668502/v1

License: This work is licensed under a Creative Commons Attribution 4.0 International License.
Read Full License

Additional Declarations: No competing interests reported.

Abstract

Marine sponges and their associated bacteria, particularly *Streptomyces* species, represent promising sources of bioactive secondary metabolites. This study focused on the isolation and characterization of proline-based 2,5-diketopiperazines (DKPs) from *Streptomyces canescens* strain AHL19 associated with the marine sponge *Haliclona caerulea* collected from the Persian Gulf. The antibacterial assay showed that the ethyl acetate culture extract of strain AHL19 inhibited the growth of pathogenic bacteria including *Staphylococcus aureus*, *Micrococcus luteus*, *Escherichia coli*, *Pseudomonas aeruginosa* with MIC values ranged from 64 to 256 µg/mL. This ethyl acetate culture extract was partitioned in water-dichloromethane that the later fraction showed potent cytotoxicity against HT29 cell lines with IC_{50} value of 4.0 ± 0.7 µg/mL and was selected for further fractionation. Six DKPs; cyclo (L-Pro-L-Val) (**1**), cyclo (L-Pro-L-Ile) (**2**), cyclo (L-Pro-L-Leu) (**3**), cyclo (L-Pro-L-Phe) (**4**), cyclo (L-Pro-L-Tyr) (**5**), and cyclo (4-hydroxy-L-Pro-L-Phe) (**6**) were isolated and their structures elucidated using LC-ESI-MS, 1D and 2D NMR. Molecular docking analysis of 2,5-DKPs against dihydrofolate reductase (DHFR) and *β*-tubulin showed that compound **5** can effectively target these proteins. MD simulation of compound **5** compared to streptomycin demonstrated that the **5**-DHFR complex exhibits greater structural stability, lower RMSD fluctuations, and more persistent key interactions throughout the 100-ns trajectory. MD calculation also revealed that compound **5** can effectively form stable interactions with cancer related target *β*-tubulin. These proline-based DKPs with proved conformational rigidity and varying degrees of antibacterial and cytotoxicity effects, are promising and potential molecules as drug leads. This is the first report of such DKPs from *H. caerulea* associated *Streptomyces*, underscoring the untapped biodiversity of marine symbionts for sustainable antibiotic and anticancer discovery.

1. Introduction

Haliclona is a genus of marine sponges belonging to the family Haliclonidae, the order Haplosclerida, and the class Demospongiae, recognized for producing a broad range of bioactive compounds with significant potential in medicine (Liang et al., 2025). These sponges are known to harbor diverse bacterial communities, particularly *Actinobacteria*, *Alphaproteobacteria* and *Firmicutes*, which contribute to the production of cytotoxic, antibacterial, antifungal and anti-inflammatory metabolites (Kim et al., 2025). The extracted metabolites from *Haliclona* have shown selective cytotoxicity against cancer cells, including apoptosis induction by compounds such as neviotin A (Saquib et al., 2023), and antimicrobial effects against resistant pathogens like *Mycobacterium* spp. through agents like haliclonacyclamines (Arai et al., 2009). Despite their promising medicinal applications, the research on *Haliclona* is accompanied by challenges, including limited availability of certain species and complexities in the drug development process. Nevertheless, ongoing advancements in microbial research methodologies aim to unlock the full therapeutic potential of *Haliclona* and its associated bacteria, offering a sustainable way for the exploration of new treatments for various diseases (Jung et al., 2022, Mehbub et al., 2024).

The natural peptides 2,5-diketopiperazines (DKPs), are the simplest and smallest form of cyclic dipeptides. These neglected structures were considered to be only protein artifacts or degradation

products, but now are recognized as structurally diverse molecules with significant therapeutic potential and privileged structures with the ability to bind to a wide range of receptors (Bojarska et al., 2021, Giessen and Marahiel, 2015). DKPs are mainly biosynthesized through two enzymes, non-ribosomal peptide synthetases and tRNA-dependent cyclodipeptide synthases (Giessen and Marahiel, 2015, Otsuka et al., 2019) by a large variety of living organisms and conserved in bacteria to humans (Huang et al., 2010) (De Rosa et al., 2003) (Ying et al., 2018).

The genus *Streptomyces* are widely distributed in marine environments and produce DKPs (Huang et al., 2014). From bioassay-guided fractionation of fermentation broth of *Str. nigra* strain 452^T eight proline-based DKPs with different cytotoxic activity were identified including cyclo (Pro-Ala), cyclo (Pro-Gly), cyclo (Pro-Phe), cyclo (Pro-Met), cyclo (Pro-Val), cyclo (Pro-Leu), cyclo (Pro-Tyr), and cyclo (L-Leu-trans-4-hydroxy-L-Pro). The highest cytotoxicity was exhibited against A549 cells by cyclo (Pro-Ala) and cyclo (Pro-Met), and against HCT-116 cells by cyclo (Phe-Pro) and cyclo (Pro-Ala), with IC_{50} values of 18.5, 27.3, 32.3, and 47.6 mg/mL, respectively (Chen et al., 2018).

In another study, bioassay-guided fractionation for low toxic antifouling metabolites from deep-sea sediment bacterium *Str. fungicidicus*, afforded five DKPs including cyclo-(L-Leu-L-Pro), cyclo-(L-Phe-L-Pro), cyclo-(L-Val-L-Pro), cyclo-(L-Trp-L-Pro), and cyclo-(L-Leu-L-Val). These antifouling compounds inhibited 50% larval attachment of the barnacle *Balanus amphitrite* with the effective concentration EC_{50} values after 24 h of 0.15, 0.28, 0.10, 0.13, and 0.27 mM, respectively. Cyclo-(L-Val-L-Pro) showed the lowest EC_{50} and the highest therapeutic ratio (LC_{50}/EC_{50}) of 7.5. They suggest DKPs and other compounds from deep-sea bacteria may be used as novel antifoulants (Li et al., 2006).

A new DKP, actinozine A or cyclo (2-OOH-D-Pro-L-Leu)] with an unprecedented hydroperoxy moiety, together with cyclo (2-OH-D-Pro-L-Leu), cyclo (D-Pro-L-Phe) and cyclo (L-Pro-L-Phe) were identified from a sponge-derived *Streptomyces* sp. Call-36. These DKPs exhibited different cytotoxicity against HCT-116 and MCF-7 cell lines and cyclo (D-Pro-L-Phe) with IC_{50} values of 32.7 and 81.9 μM, respectively and actinozine A showed antimicrobial effects against *Staphylococcus aureus* and *Candida albicans* with inhibition zones of 23 and 19 mm at 100 μg/disc, respectively, highlighting the potential of marine *Streptomyces* for bioactive metabolites (Shaala et al., 2019). Proline-phenylalanine DKP, *cis*-cyclo-(L-Phe-L-Pro), was isolated through bioassay-guided fractionation for antibacterial compounds from the culture extract of novel *Bacillus horneckiae*-like strain 2011SOCCUF3, associated with the marine sponge *Spongia officinalis*.(Obled et al., 2025)

DKPs especially proline-based DKPs have diverse biological properties such as antioxidant, neuroprotective, anticancer, antimicrobial, and immunomodulatory effect, and metabolic and cardiovascular benefits (Bojarska et al., 2021). Moreover, proline- and hydroxyproline-derived DKPs have emerged as novel quorum-sensing inhibitors, playing key roles in intracellular communication (Sun et al., 2020). Additionally, these compounds show promise in the prevention of neurodegenerative disorders, such as Alzheimer's and Parkinson's diseases (Turkez et al., 2020). Proline-based DKPs core has unique structure due to the fusion of a piperazine nucleus with a pyrrolidine ring, which imparts a highly rigid

heterocyclic structure and conformational stability and enhances bioavailability and receptor binding, which resulting in eminent biological activities that was mentioned earlier (Bojarska et al., 2020, Song et al., 2021) .

There are reviews that consider the sources and biological activities of DKPs from natural sources (Borthwick, 2012, Liang et al., 2023, Song et al., 2021). A comprehensive review has summarized the occurrence, enzymatic synthesis, and diverse pharmacological properties of DKPs, as well as their potential applications in food and medicine (Fizza et al., 2025). In another review, cyclo (L-Leu-L-Pro) known as gancidin W is introduced as a widespread DKPs in nature that has been identified in about 60 bacterial species notably belonging to *Bacillus*, *Pseudomonas*, and *Streptomyces* genera, and also generally in combination with other DKPs exhibiting antimicrobial, anticancer, antiviral, neuroprotective activities and as a quorum-sensing modulator (Bailly, 2025).

Zhu et al (2019), reviewed the bioactive nitrogenous secondary metabolites from *Haliclona* genus and reported that as many as 103 alkaloids have been isolated and characterized from *Haliclona* sponges since 1994 and only eight alkaloids have been separated from *Haliclona* sponge-derived microbes until that time (Zhu et al., 2019). Among them cyclo (L-Pro-D-Leu) and cyclo (L-Pro-D-Val) isolated from the ethyl acetate extract of the strain *Bacillus megaterium* LC3CS2 symbiont of the sponge *Haliclona oculata* collected from Son Cha Peninsula in Vietnam (Cuong et al., 2014). However, DKPs are common, there is no report on proline-based DKPs from the sponge *Haliclona*-associated *Streptomyces*, and it remains underexplored till now.

Searching for new antibiotics due to the rising resistance and the need for sustainable sources motivated us to explore additional antibiotic agents from the biodiversity of marine-associated microorganisms (Alborz et al., 2025). Since marine sponges and their associated bacteria, particularly *Streptomyces* species, are valuable sources of antibacterial compounds, we isolated and characterized bioactive compounds from the most potent antibacterial extract of *Haliclona*-associated bacteria using modern isolation techniques and structural elucidation methods, including LC-ESI-MS, together with 1D and 2D NMR. Preliminary cytotoxic and antibacterial assessments were conducted on all sponge *Haliclona caerulea* associated bacterial extracts, and the most potent extract which was *Str. canescens* selected for further study. Six proline-based 2,5-diketopiperazines were isolated and characterized from *Str. canescens* fermentation broth.

2. Materials and Methods

2.1. Isolation, cultivation, and extraction of sponge-associated bacteria

Sponge sample collection and isolation of associated bacteria

Marine sponge, *Haliclona caerulea* (Porifera, Class Demospongiae, Order Haplosclerida, Family Chalinidae) was collected from the depth of 3–5 meters of coastal waters of Larak Island, Persian Gulf, using scuba diving in autumn 2020. Sponges were identified by the taxonomist, Dr. Melika Nazemi after collection(Alborz et al., 2025). To avoid contamination and preserve the integrity of the sponge microbiome, the sponge samples were transferred to sterile plastic containers on ice to laboratory for isolation of their bacteria (Nazemi et al., 2017) A voucher specimen (number HC-1047) was deposited in the sponge collection at the Persian Gulf and Oman Sea Ecological Research Institute.

The collected samples were rinsed using sterile seawater, and subsequently sectioned, homogenized, and serially diluted in sterile seawater. A volume of 100 µL of each dilution was cultured on starch-yeast extract peptone agar (SYPA) and marine sponge agar (MSA) media (Ansarizadeh et al., 2023, Gozari et al., 2019). The cultured media were kept at 28°C for 4 weeks for incubation. The colonies were sub-cultured to the same media and checked with observation under a microscope and macroscopically (Pourmozaffar et al., 2023, Alborz et al., 2025).

Production and extraction of the bacterial secondary metabolites

The isolated bacteria were inoculated in a fermentation medium containing 10 g/L malt extract, 8 g/L starch, 1 g/L tryptone, 3 g/L yeast extract, 2 g/L glycerol prepared in filtered natural seawater at pH 7.3. The Erlenmeyer flaxes were placed in a shaking incubator (220 rpm) for 5 days at 28°C (Gozari et al., 2018). Subsequently, the fermented medium was filtered through Whatman No. 1 filter paper and was extracted with equal volume of ethyl acetate twice. Then, the ethyl acetate layer was evaporated under reduced pressure at 40°C to produce a dried crude extract. The resulted crude extracts from the isolated bacteria were kept at − 70°C for further experiments (Gozari et al., 2018).

Mass production and extraction of secondary metabolites from Streptomyces sp. strain AHL19

The strain AHL19 was selected for mass production based on the results of cytotoxicity, antibacterial activity, TLC, HPLC, and LC-MS chromatograms. The seed medium (100 mL) was inoculated with 5 mL of the AHL19 strain spore suspension (5×10^9 spores/mL). Seed medium containing 10 g/L soluble starch, 2 g/L K_2HPO_4, 2 g/L KNO_3, 0.3 g/L casein, 0.05 g/L $MgSO_4.7H_2O$ in 1 liter filtered natural seawater at pH 7.0. Subsequently, the seed medium was incubated at 28°C for 48 hours. Then, 10% of seed medium was inoculated into 15 liters of optimized production medium (5 batches). The production medium was incubated for 6 days at 28°C in a shaking incubator (220 rpm) for each batch. After termination of fermentation period, the broth was collected and extracted by the equal volume of ethyl acetate twice.

2.2 Bioactivity Screening

Cytotoxicity evaluation of fractions from AHL19

The cytotoxicity of different fractions of AHL19 was tested against HT29 cells by MTT reduction assay (Zare et al., 2020). Human colorectal adenocarcinoma cell line HT29 was obtained from National Cell Bank of Iran (Pasteur Institute of Iran, Tehran) and Iranian Biological Resource Center, Tehran, Iran. The

HT29 cells were cultured in RPMI1640, supplemented with 10% FBS, 100 IU/mL penicillin and 100 mg/L streptomycin and grown at 37°C in humidified air containing 5% CO_2. One-hundred µL of cell suspensions of HT29 cells with a density of 2×10^4 cells/mL were transferred to each well of a 96-well microplate. After incubation at 37°C for 24 h, the cultured cells were treated with 100 µL of each fraction at final concentrations of 500, 100, 20, 4 µg/mL. Then HT29 cells were incubated with the fractions for 36 and 72 hours. After the incubation period, 50 µL of the MTT solution at concentration of 0.5 mg/mL was placed in each well and incubated for further 4 h. The media was then removed and 100 µL of a DMSO: ethanol (4:1) solution was added to each well to solubilize the formazan crystals. Finally, the absorbance of each well was measured at λ 570 nm using a microplate reader. The percentage of cell viability at each concentration was calculated as follows:

Cell viability (%) = $[(OD_{Test}) - (OD_{Blank})] / [(OD_{Control}) - (OD_{Blank})] \times 100$

The blank control (OD_{Blank}) is the absorbance of the medium. IC_{50} values defined as the concentration of the sample that inhibits the viability of cells at 50%, were calculated by Curve Expert software version 1.3 for Windows.

Screening of antibacterial activity using minimum inhibitory concentrations method

The minimum inhibitory concentrations (MICs) of the extracted metabolites from the AHL19 isolate were assessed against the bacterial strains *Staphylococcus aureus* (ATCC 9144), *Micrococcus luteus* (ATCC 9341), *Escherichia coli* (ATCC 25922), *Pseudomonas aeruginosa* (ATCC 27853) according to the standard microdilution protocol CLSI 2015 (Jorgensen and National Committee for Clinical Laboratory Standards, 1997). The stock concentration of crude extract was prepared in 5% dimethyl sulfoxide (Molecular biology grade) and diluted by twofold serially dilution method to final concentrations (1024, 512, 256, 128, 64, 32 and 16 µg/ml). Streptomycin was used as the standard positive control. Each well was inoculated with 5 µl of 10^8 CFU/mL of the bacterial suspensions. The inoculated 96 well plates were incubated for 24 hours at 37°C for bacterial growth. Following the incubation period, absorbance was determined at 550 nm using a microplate reader (BioTek® Instruments). The MIC values of the extracts were evaluated according to the lowest concentration of an extract that prevented the growth of the test strains.

2.3 Bacterial Identification and Characterization

Morphological, biochemical, and physiological characterization

The morphology and arrangement of spore chains and aerial hyphae of the AHL19 isolate was analyzed on ISP 2 agar medium for 14 days at 28°C by coverslip method (Kawato and Shinobu, 1959). The AHL19 was characterized physiologically and biochemically using International Streptomyces Project (ISP) media (Shirling and Gottlieb, 1966). Carbon source consumption was assessed by culturing the cytotoxic strains in ISP-9 medium supplemented with 1% of various carbon sources. Hydrogen sulfide production, diagnostic enzyme tests, and the assimilation of nitrogen sources were assessed using the Williams

method (1989) (Williams, 1989). The determination of growth temperature ranges and salinity tolerance of AHL19 isolate was conducted on ISP-2 medium.

Molecular characterization and phylogenetic analysis

The genomic DNA of AHL19 isolate was extracted using the CTAB procedure (Kieser et al., 2000). Then, its 16S rRNA gene was PCR-amplified with universal primers 27F and 1492R (Heuer et al., 1997), and the purified product was sequenced by Pishgam Biotech Company (Tehran, Iran). The 16S rRNA sequence was compared to GenBank 16S rRNA genes using the Blastn program (Zhang et al., 2000). The 16S rRNA sequence was aligned for phylogenetic analysis, and the phylogenetic dendrogram (Fig. 1) was constructed using the MEGA X program, employing the neighbor-joining method.

2.4 Chemical Analysis and Fractionation

Chemicals and analytical instruments

The NMR spectra were recorded on a Bruker BioSpin GmbH instrument operating at 600 and 150 MHz for ^{1}H and ^{13}C NMR, respectively. The NMR were measured in deuterated methanol (CD_3OD) and chemical shifts were expressed in parts per million (δ) downfield from tetramethylsilane (TMS) as an internal standard. Chemical shifts were reported with reference to the respective solvent peaks (δ_H 3.30 and δ_C 49.0 for CD_3OD). Coupling constants (*J*) are reported in hertz (Hz). The 2D NMR experiments ($^{1}H–^{1}H$ COSY, HETCOR, and HMBC) were performed using standard Bruker software.

HPLC-Diode Array Detector-Electro Spray Ionization Mass Spectroscopy (LC-DAD-ESI-MS) were measured on Shimadzu LCMS- 2010EV system equipped with an SPD-M20A photo DAD and an ESI mass in the positive and negative modes. A RP-18 Phenomenex Luna column, 5 µm, 250 × 10 mm ID axial with pre-column 10 × 10 mm, and LC pump (LC 20 AD) with flow rate 0.25 mL/min was used.

The analytical HPLC system was a Knauer Azura with (p 6.1 L) pump and a Knauer Ultraviolet detector (2.1 L) with a column Eurospher-100 C18 (Eurospher-100 C18, 250 × 4.6 mm, Knauer, Germany). Semi-preparative HPLC separations were developed on a Knauer system that consisted of a K-1050 pump, an RP-18 (Phenomenex Luna, 5 µm, 250 × 10 mm ID axial with pre-column 10 × 10 mm ID) column, and with a four-channel K-2600 UV detector set at λ 210, 230, 254 and 320 nm. Thin-layer chromatography (TLC) was carried out on pre-coated aluminum plates silica gel 60 F_{254}, Merck, and spots were visualized by spraying with anisaldehyde /sulfuric acid followed by heating to 120 °C. The HPLC grades solvents, methanol (MeOH), acetonitrile (MeCN), dichloromethane (DCM), ethyl acetate, and *n*- hexane were obtained from Merck (Darmstadt, Germany).

Liquid-liquid extraction of Haliclona-associated bacteria extracts into n-hexane, DCM, and aq. MeOH fractions

The crude extracts of strain AHL19 were partitioned using Liquid-Liquid Extraction (LLE). The ethyl acetate extract was dissolved in MeOH: water (9:1 v/v) to prepare the mother solution, which was then

successively partitioned between two solvents, *n*-hexane and DCM, in order of increasing polarity. The resulting fractions were dried by evaporating the respective solvents using a rotary evaporator to yield *n*-hexane, DCM and aqueous-MeOH fractions. All fractions were stored at 4°C until further analysis.

Purification of DCM fraction of AHL19 extract

Based on chemical profile and cytotoxicity assessment results of fractions obtained from *Streptomyces* sp. AHL19 (Fig. S3), the DCM fraction showed a distinct chemical profile and strong inhibition against the HT29 cell line, with an IC_{50} value of 4.0 ± 0.7 µg/ml. Therefore, this strain was selected for further fractionation.

The DCM fraction was first analyzed by analytical HPLC to determine the analytical condition using an RP-C18 column in gradient elution consisting of MeCN and H_2O as the following solvent gradient program, 10% to 60% MeCN in ultrapure water and flow rate of 1.0 mL/min. Purification of DCM fraction was performed with semi-preparative RP-C_{18} HPLC (Phenomenex RP18 250 × 10 mm. MeCN-H_2O, 15:85, v/v; 4 mL/min, 35 min), to yield 6 pure compounds (Fig. S4). The purity of the compounds was re-checked by analytical HPLC and submitted for Mass and NMR spectroscopy analyses (Fig. S5).

LC-MS screening of DCM and aq. MeOH fractions of strains AHL19

According to cytotoxicity of DCM and *aq.* MeOH fractions of strain AHL19, these fractions were analyzed by LC-MS technique. The DCM fraction of strain AHL19 bacteria was loaded onto an RP-C18 UPLC (Acetonitrile (solvent B) – 0.1% formic acid in H_2O (solvent A), 5%–95%) to observe main compounds (Fig. S6). The gradient method was: 5% B in initial time; 5% to 95% B in 45 min; 100% B in 15 min; 95% to 5% B in 10 min. The injection volume was 10 µL and detection was at λ 254 nm.

Spectral data of pure compounds **1**–**6** *from DCM fraction of AHL19 extract*

Cyclo (L-Proline-L-Valine) (SMILES: CC(C)[C@H]1C(= O)N2CCC[C@H]2C(= O)N1, **1**), ESI-MS *m/z* 197.2 $[M + H]^+$ ($C_{10}H_{16}N_2O_2$). ^{1}H NMR (600 MHz, CD_3OD): δ_H 4.10 (1H, t, *J* = 7.2 Hz, H-6), 3.94 (1H, s, H-9), 3.46 (1H, dt, *J* = 11.8, 7.7 Hz, H-3a), 3.40 (1H, ddd, J = 11.8, 8.6, 3.2 Hz, H-3b), 2.40 (1H, hept, *J* = 7.0 Hz, H-10), 2.23 (1H, m, H-5a), 1.93 (1H, m, H-4a), 1.85 (1H, m, H-5b), 1.83 (1H, m, H-4b), 1.00 (3H, d, *J* = 7.0 Hz, H-11), 0.83 (3H, d, *J* = 7.0 Hz, Me-10); broad s at 4.48 (1H, NH). ^{13}C NMR (150 MHz, CD_3OD): δ_C 171.2 (C-7), 166.1 (C-1), 60.0 (C-9), 58.7 (C-6), 44.5 (C-3), 28.4 (C-10), 28.1 (C-5), 21.7 (C-4), 17.2 (C-11), 15.2 (Me-10) (He et al., 2013).

Cyclo (L-Proline-L-Isoleucine) (SMILES: CC[C@H](C)[C@H]1C(= O)N2CCC[C@H]2C(= O)N1, **2**), ESI-MS *m/z* 211.3 $[M + H]^+$ ($C_{11}H_{18}N_2O_2$). ^{1}H NMR (600 MHz, CD_3OD): δ_H 4.10 (1H, dd, *J* = 9.5, 6.5 Hz, H-6), 3.97 (1H, br s, H-9), 3.46 (1H, dt, *J* = 13.1, 8.2 Hz, H-3a), 3.40 (1H, tt, *J* = 8.9, 4.4 Hz, H-3b), 2.23 (1H, m, H-5a), 2.06 (1H, m, H-10), 1.93 (1H, m, H-4a), 1.84 (2H, m, H-4b/H-5b), 1.34 (1H, m, H-11a), 1.22 (1H, m, H-11b), 0.97 (3H, d, *J* = 7.1 Hz, Me-10), 0.83 (3H, t, *J* = 7.5 Hz, H-12); broad s at 4.50 (1H, NH). ^{13}C NMR (150

MHz, CD_3OD): δ_C 171.0 (C-7), 166.1 (C-1), 60.0 (C-9), 58.5 (C-6), 44.6 (C-3), 35.7 (C-10), 28.0 (C-5), 24.0 (C-11), 21.7 (C-4), 14.0 (Me-10), 11.0 (C-12) (Noël et al., 2017).

Cyclo (L-Proline-L-Leucine) (SMILES: O=C1N2[C@](C(= O)N[C@H]1CC(C)C)(CCC2)[H], **3**), ESI-MS *m/z* 211.3 $[M + H]^+$ ($C_{11}H_{18}N_2O_2$). ^1H NMR (600 MHz, CD_3OD): δ_H 4.16 (1H, t, *J* = 7.9 Hz, H-6), 4.03 (1H, dd, *J* = 9.1, 3.4 Hz, H-9), 3.41 (2H, dd, *J* = 8.5, 3.6 Hz, H-3), 2.20 (1H, dt, *J* = 10.1, 6.3 Hz, H-5a), 1.92 (1H, m, H-5b), 1.91 (1H, m, H-4a), 1.84 (1H, m, H-4b), 1.81 (1H, m, H-10a), 1.78 (1H, m, H-11), 1.42 (1H, m, H-10b), 0.86 (6H, d, *J* = 6.6 Hz, Me-11/Me-10). ^{13}C NMR (150 MHz, CD_3OD): δ_C 171.5 (C-7), 167.6 (C-1), 58.8 (C-6), 53.2 (C-9), 45.0 (C-3), 37.8 (C-10), 27.5 (C-5), 24.4 (C-11), 22.3 (C-4), 21.0 (Me-11/Me-10, overlapping) (He et al., 2013).

Cyclo (L-Pro-L-Phe) (SMILES: O=C1N[C@@H](Cc2ccccc2)C(= O)N2CCC[C@@H]12, **4**): ESI-MS *m/z* 245.3 $[M + H]^+$ ($C_{14}H_{16}N_2O_2$). ^1H NMR (600 MHz, CD_3OD): δH 7.15 (5H, m, Ar-H), 3.97 (1H, dd, J = 11.1, 6.3 Hz, H-6), 3.40 (1H, tt, *J* = 8.9, 4.4 Hz, H-3a), 3.25 (1H, m, H-3b), 4.35 (1H, t, *J* = 5.0 Hz, H-9), 3.05 (1H, t, *J* = 5.0 Hz, H-10a), 2.99 (1H, dd, *J* = 14.2, 5.2 Hz, H-10b), 1.84 (1H, m, H-4a), 1.70 (1H, m, H-4b), 2.00 (1H, m, H-5a), 1.12 (1H, m, H-5b). ^{13}C NMR (150 MHz, CD_3OD): δ_C 171.5 (C-7), 167.6 (C-1), 136.0 (C-1'), 129.5 (C-2'/6'), 127.9 (C-3'/5'), 126.6 (C-4'), 58.8 (C-6), 53.2 (C-9), 45.0 (C-3), 37.8 (C-10), 27.5 (C-5), 22.3 (C-4) (Noël et al., 2017).

Cyclo (L-Pro-L-Tyr) (SMILES: C1C[C@H]2C(= O)N[C@H](C(= O)N2C1)CC3 = CC = C(C=C3)O; **5**): ESI-MS *m/z* 261.3 $[M + H]^+$ ($C_{14}H_{16}N_2O_3$). ^1H NMR (600 MHz, CD_3OD): δH 6.95 (2H, d, *J* = 8.1 Hz, H-3'/5'), 6.60 (2H, d, *J* = 8.1 Hz, H-2'/6'), 4.26 (1H, t, *J* = 5.1 Hz, H-9), 3.95 (1H, dd, *J* = 11.2, 6.3 Hz, H-6), 3.45 (1H, dt, J = 12.0, 8.5 Hz, H-3a), 3.25 (1H, m, H-3b), 2.99 (1H, dd, *J* = 14.2, 5.2 Hz, H-10a), 2.93 (1H, dd, *J* = 14.2, 4.6 Hz, H-10b), 2.00 (1H, dq, *J* = 11.2, 5.4 Hz, H-5a), 1.70 (2H, m, H-4), 1.13 (1H, td, *J* = 21.3, 10.8 Hz, H-5b); broad s at 4.48 (2H, NH/OH). ^{13}C NMR (150 MHz, CD_3OD): δ_C 169.8 (C-7), 165.6 (C-1), 156.4 (C-4'), 130.7 (C-2'/6'), 126.8 (C-1'), 114.6 (C-3'/5'), 58.6 (C-6), 56.4 (C-9), 44.6 (C-3), 36.2 (C-10), 27.9 (C-5), 21.3 (C-4) (Sunaryanto et al., 2011).

Cyclo (4-Hydroxy-L-Proline-L-Phenylalanine) (SMILES: C1[C@H](CN2[C@@H]1C(= O)N[C@H](C2 = O)CC3 = CC = CC=C3)O; **6**), ESI-MS *m/z* 261.3 $[M + H]^+$ ($C_{14}H_{16}N_2O_3$), noting OH group on proline moiety. ^1H NMR (600 MHz, CD_3OD): δ_H 7.18 (2H, m, H-3'/5'), 7.14 (2H, m, H-2'/6'), 7.13 (1H, m, H-4'), 4.39 (1H, br t, J = 6.3 Hz, H-9), 4.27 (1H, dd, J = 12.0, 6.0 Hz, H-6), 4.17 (1H, br t, J = 5.1 Hz, H-4), 3.61 (1H, dd, J = 13.2, 5.1 Hz, H-3a), 3.20 (1H, m, overlaps solvent, H-3b), 3.07 (2H, t/m, J = 5.2/5.8 Hz, H-10), 1.97 (1H, dd, J = 13.2, 6.0 Hz, H-5a), 1.27 (1H, td, J = 12.0, 5.1 Hz, H-5b); broad s at 4.50 (2H, NH/OH). ^{13}C NMR (150 MHz, CD_3OD): δ_C 169.7 (C-7), 165.7 (C-1), 136.0 (C-1'), 129.5 (C-2'/6'), 127.9 (C-3'/5'), 126.6 (C-4'), 67.1 (C-4), 56.8 (C-6), 56.1 (C-9), 53.6 (C-3), 37.5 (C-5), 36.5 (C-10) (Noël et al., 2017).

2.5 Computational study

Molecular docking study

The essential target enzymes established by previous studies were used to assess the chemical activities of the chemicals included in the fractures. These enzymes are DNA gyrase A (El-Saghier et al., 2025) (PDB ID: 5IWI), DNA gyrase B (Shafiq Osw et al., 2024) (PDB ID: 3U2D), and Dihydrofolate reductase (DHFR) (Sahiba et al., 2024) (PDB ID: 3SRW). In addition to these targets that are related to the antibacterial effect of the compounds, a target was also selected to evaluate the anticancer activity of the compounds. Based on the previous studies, proline-based 2,5-DKPs have been reported to exert their anticancer activity primarily through binding to the colchicine-binding site of *β*-tubulin (Tian et al., 2018). Therefore, (PDB ID: 5C8Y) was also used as one of the potential targets. The protein structure was constructed using the Schrödinger Suite's protein preparation module after being obtained from the PDB database (http://www.rcsb.org/pdb). The water molecules were eliminated and the missing hydrogen atoms were added. Following the creation of an H-bond network, the OPLS force field was used to minimize the system (Poustforoosh and Elyasi). The co-crystallized ligand was used to identify the protein's active binding site, and a receptor grid was created around the active region to produce more reliable results (Poustforoosh, 2025). The compounds' structures were sketched and stored in SDF format. The Schrödinger LigPrep module was used to create the precise protonation states for ligands. Finally, the Glide of Schrödinger suites were used to operate molecular docking.

Molecular dynamics (MD) simulation

Dynamically, the interactions between the antibacterial control molecule and the ligand-protein with the highest binding affinity were also evaluated. The MD simulation was carried out using Desmond of Schrödinger. For the MD, the ligand-protein complex derived from the docking calculations was utilized. The solvent model of transferable intermolecular potential with three points (TIP3P) was selected for the simulations, which were carried out in an orthorhombic box (Poustforoosh, 2026). The Schrödinger system setup was utilized to neutralize the system using the appropriate quantity of Na+/Cl− ions and a salt concentration of 0.15 M (Sirin et al., 2014). The simulation was then run for 100 ns using the constant number of atoms, pressure, and temperature (NPT) ensemble and the software's default relaxation technique (Poustforoosh et al., 2025). The temperature was set to 310.15 K (37°C) using the Nose-Hoover technique, and isotropic scaling was employed to bring the pressure down to 1 atm (Panwar and Singh, 2021).

3. Results and discussion

3.1 Isolation of sponge-associated bacteria

The bacterial isolate was derived from the sponge *Haliclona caerulea* samples. The bacterial isolate was coded according to the collection season (Autumn), the source (*Haliclona*) and the location (Larak Island). The results of preliminary characterization based on some morphological, biochemical, and physiological characteristics showed that the isolated bacteria were belonged to *Streptomycetaceae* family.

3.2 Antibacterial activity assays

The antibacterial activity of the bacterial isolate AHL19 was assessed, and the results demonstrated potent activity. Determination of minimum inhibitory concentration (MIC) values of the AHL19 ethyl acetate extracts showed broad-spectrum activity against both Gram-positive and Gram-negative bacteria, ranging from 64 to 256 µg/mL (Table 1).

Table 1
Antibacterial activity of the ethyl acetate extracted metabolites from the isolated bacterial strain AHL19

Isolates	**Minimum inhibitory concentration (µg/mL)**			
	S. aureus	***M. luteus***	***E. coli***	***P. aeroginosa***
AHL19	64	64	128	256
Streptomycin	8	8	8	16

3.3 Identification of AHL19

Morphological, biochemical and physiological characterization

After preliminary characterization of the isolate, including morphological and chemotaxonomic analyses, we identified AHL19 isolate according to biochemical, physiological and molecular methods. The cultural characteristics of the spore chains of AHL19 were spirals type. The chemo-taxonomical investigation revealed that AHL19 isolate contained LL-diaminopimelic acid without diagnostic sugars in their cell wall hydrolysates. Biochemical and physiological experiments showed that AHL19 isolate utilized glucose, fructose, xylose, arabinose and mannitol as sole carbon sources and could not grow on raffinose.

The nitrogen utilization experiment demonstrated that the AHL19 isolate used arginine, valine and asparagine as sole nitrogen source and could not assimilate ornithine. In addition, AHL19 isolate produced diffusible pigment. AHL19 were mesophilic and produced the catalase and nitrate reductase enzymes, whereas it could not produce hydrogen sulfide and oxidase. This isolate could grow at pH 5–9 whereas and it tolerated NaCl concentration up to 10% (Table 2).

Molecular characterization and phylogenetic analysis

Analysis of the 16S rRNA gene sequences using BLAST software exhibited different similarity ranges between AHL19 isolate and the type strains in the NCBI database. AHL19 isolate showed high similarity (> 99%) with *Streptomyces canescens.* Interpretation of the constructed phylogenetic tree based on 16S rRNA gene demonstrated that the selected strains positioned in two different clades and they shared sub clades by their closest type strains. The AHL19 isolate located in different clades and lineage along with the most similar strain of *S. canescens* (Fig. 1).

Table 2
Morphological, physiological and biochemical characterization of cytotoxic AHL isolates

Characters		**AHL19**
Color	Vegetative mycelia	Red
	Aerial mycelia	Gray
Growth and sporulation on	ISP II	Good
	ISP III	Low
	ISP IV	Good
	ISP V	Good
	ISP VI	Good
	ISP VII	Good
	CDA	Good
	BA	Good
	NA	Low
Spore morphology		Spirals
Melanoid pigment		-
Diffusible pigment		-
Carbon sources utilization	Glucose	+
	Fructose	+
	Xylose	+
	Arabinose	+
	Rhamnose	-
	Sucrose	-
	Raffinose	-
	Galactose	+
	Manitol	+
	Inositol	-
Nitrogen sources utilization	Valine	+
	Arginine	+

Characters		AHL19
	Ornithine	-
	Asparagine	+
DAP-isomer		LL
Whole cell sugar		ND
Growth temperature range		10–45°C
Growth pH range		5–9
H_2S production		-
Catalase production		+
Oxidase production		-
Nitrate reduction		+
NaCl Tolerance		< 10%

3.4 TLC, HPLC, and LC-MS screening of bacterial extracts

The *Haliclona*-associated bacterial strain AHL19 (200 mg) was analyzed by different chromatographic techniques such as TLC, HPLC and LC-MS analyses. The bacterial ethyl acetate crude extract was subjected on silica gel F_{254} TLC using *n*-hexane: ethyl acetate and also ethyl acetate: MeOH as mobile phase (Fig. S1). Considering different low, medium and high polarity of mobile phase through the TLC, AHL19 strain consists of moderate to polar metabolites. For further investigation, reversed-phase (RP-C_{18}) HPLC analysis was used and HPLC column eluted with MeCN (20% to 100% in 50 min) in ultrapure water.

According to the results of TLC and HPLC analysis (Fig. S1, S3A), liquid-liquid extraction (LLE) was recommended for further investigation of the extract. Therefore, the crude extract was partitioned through LLE by a modified Kupchan method (Kupchan, 1970). The extract yielded *n*-hexane (2.5 mg), dichloromethane (DCM, 6.0 mg) and aq. MeOH (3.7 mg) fractions, which were analyzed further by silica gel F_{254} TLC as well (Fig. S2). The TLC analysis of partitioned fractions showed that the separation was effective and AHL19 showed diverse metabolites.

3.5 Cytotoxic activity of fractions from AHL19 strain

Cytotoxic activity of *n*-hexane, DCM, and aq. MeOH fractions of AHL19 was tested against HT29 cell line using MTT assay. The results showed that aq. MeOH and DCM fractions exhibited high cytotoxic activity against HT29 cells, which were further investigated (Table 3).

Table 3
Cytotoxic activity (IC_{50} ±SE (µg/mL) of fractions from *H.caerulea* AHL19 symbiosis bacteria strain against the HT29 cell line.

Fractions of AHL19	IC_{50} ±SE (µg/mL)
n-hexane	30.3 ± 7.8
DCM	4.0 ± 0.7
aq. MeOH	1.9 ± 0.3

3.6 Structure elucidation of cyclodipeptides 1–6 from DCM fraction of AHL19

Six proline-based diketopiperazines (DKPs) or cyclic dipeptides (Fig. 2) were isolated from the dichloromethane (DCM) fraction of *S. canescens* AHL19 strain, associated with the marine sponge *H. caerulea*. The structures were elucidated using 1D, ^{1}H and ^{13}C NMR, and 2D ^{1}H-^{1}H COSY, HSQC, and HMBC NMR spectroscopy (CD_3OD,600 MHz), with assignments supported by comparison to literature data for similar cyclodipeptides (Noël et al., 2017, Sunaryanto et al., 2011). The structural identification was explained for cyclo (L)-Pro-(L)-Val (**1**) and another proline-based DKPs with aromatic amino acid, cyclo (L)-Pro-(L)-Tyr (**5**).

The ^{1}HNMR and ^{13}CNMR for all compounds are presented in Table S1 and S2 (except for ^{13}CNMR of **4**), and all 1D and 2D NMR spectrum are reported in supplementary materials (Fig. S7-S27). The COSY and key HMBC correlations are illustrated in Fig. 3.

Key features included characteristic signals for the 2,5-DKP ring with two amide carbonyls, C-1 and C-7, at δ_C 165–172 ppm, the proline pyrrolidine ring with methylene carbons at δ_C 21–45 ppm, and the *α*-carbon at δ_C 58–59 ppm. Stereochemistry was assigned based on and comparison with reported ^{13}CNMR natural cyclodipeptides from *Streptomyces* spp (Sunaryanto et al., 2011, Kim et al., 2019, Noël et al., 2017, Shaala et al., 2020).

Compound **1** was obtained as a white amorphous powder. Its LC-ESI-MS analysis in positive mode showed a protonated molecular ion peak at *m/z* 197.2 [M + H]. The ^{1}H NMR spectrum displayed characteristic signals of a proline-valine DKP, including a triplet at δ_H 4.10 ppm (1H, t, *J* = 7.2 Hz, H-6) for the proline α-proton, a singlet at δ_H 3.94 (1H, s, H-9) for the Valine α-proton, and multiplet signals for the aliphatic methylene of proline ring (δ_H 3.46, dt, *J* = 11.8, 7.7 Hz, H-3a; δ_H 3.40, ddd, *J* = 11.8, 8.6, 3.2 Hz, H-3b, δ_H 1.83, and 1.93, m, 2H, H-4a and b; δ_H 2.23, 1.85, m, 2H, H-5a and b). The valine side chain was evident from a heptet at δ_H 2.40 (1H, hept, *J* = 7.0 Hz, H-10) and two methyl doublets at δ_H 1.00 (3H, d, *J* = 7.0 Hz, H-11) and δ_H 0.83 (3H, d, *J* = 7.0 Hz, Me-10).

The ^{13}C NMR spectrum showed 10 signals, including two amide carbonyls at δ_C 166.1 (C-1) and δ_C 171.2 (C-7), confirming the DKP ring. The proline carbons were assigned as δ_C 44.5 (C-3, CH_2), δ_C 21.7 (C-4, CH_2), δ_C 28.1 (C-5, CH_2), and δ_C 58.7 (C-6, CH). The valine residue included δ_C 60.0 (C-9, CH), δ_C 28.4 (C-10, CH), δ_C 17.2 (C-11, CH_3), and δ_C 15.2 (Me-10, CH_3).

COSY correlations connected H-3 to H-4, and H-5 to H-6 in the proline ring and H-10, H-11, and Me-10 in the valine side chain. HMBC correlations from H-6 to C-1 and C-7 and also from H-9 to C-1 and C-7 confirmed the cyclodipeptide linkage. The key correlation of COSY and HMBC are shown in Fig. 3. Therefore, the structure was elucidated as cyclo (L-prolyl-L-valyl), which were previously reported from marine *Streptomyces* (Kim et al., 2019).

Compound **2** exhibited close ^{1}H NMR and ^{13}C NMR profiles to those of compound **1**, indicative of a similar DKP 5/6 membered dicyclic core. Comparative analysis revealed an additional methylene unit in the aliphatic region, consistent with the presence of an isoleucine residue in place of valine. The characteristic HMBC correlation of H-11 to the carbon atoms at C-9, C-10, C-12, and Me-10 along with COSY correlations between H-10, H-11, H-12, and Me-10 confirm the branched nature of the isoleucine side chain. Thus, based on the spectroscopic data, compound **2** was identified as cyclo (L-prolyl-L-isoleucyl). Its LC-ESI-MS analysis in positive mode showed a protonated molecular ion peak at *m/z* 211.2 $[M + H]^+$(Fig. S28).

Compound **3**, structurally analogue of **2**, shows similar ^{1}H NMR and ^{13}C NMR profiles to those of **1**. However, it differs in multiplicity of the H-9 signal (δ_H 4.03, dd, *J* = 9.1, 3.4 Hz), which is split by two protons of H-10. The isobutyl side chain displays two doublets at δ_H 0.86 with *J* values of 6.6 Hz, corresponding to the two methyl groups of C-12 and Me-11. The HMBC correlations of these two terminal methyls to C-10 and C-11 confirm the presence of a leucine residue in this structure. LC-ESI-MS analysis in positive mode revealed a protonated molecular ion peak at *m/z* 211.3 $[M + H]^+$(Fig. S29). Based on these spectroscopic data, compound **3** was identified as cyclo (L)-Pro-(L)-Leu.

For compound **4**, only the ^{1}H NMR spectrum was available, and the data were consistent with other previously reported DKPs (Noël et al., 2017). The 1H NMR spectrum revealed signals for the proline moiety, including δ_H 3.45 (1H, dt, *J* = 12.0, 8.5, 8.5 Hz) and δ_H 3.25 (1H, td, J = 12.5, 12.0, 6.5 Hz) for H-3, δ_H 1.70 (2H, m) for H-4, δ_H 2.00 (1H, m) and 1.12 (1H, m) for H-5, and δ_H 3.97 (1H, dd, *J* = 11.1, 6.3 Hz) for H-6. Two triplets at δ_H 4.35 (1H, t, *J* = 5.0 Hz) for H-9 and δ_H 3.05 (1H, t, *J* = 5.0 Hz) for H-10, along with aromatic multiplet at δ_H 7.15 (5H, m), indicated the phenylalanine residue. Its structure was assigned as cyclo(L-prolyl-L-phenylalanyl) and consistent with the study which isolated **4** from *S. fungicidicus* (Li et al., 2006).

Compound **5** was isolated as a pale yellow amorphous solid. The LC-ESI-MS in positive mode showed m/z 261.2 [M + H] (Fig. S30). $^{+}$The ^{1}H NMR spectrum revealed signals for the proline moiety, including δ_H 3.45 (1H, dt, *J* = 12.0, 8.5 Hz) and δ_H 3.25 (1H, m) for H-3, δ_H 1.91 and 1.84 (2H, m) for H-4, δ_H 2.20 (1H,

dt, *J* = 10.1, 6.3 Hz) and δ_H 1.92 (1H, m) for H-5. A doublet of doublet at δ_H 3.95 (1H, dd, *J* = 11.2, 6.3 Hz) for H-6 and a triplet at δ_H 4.26 (1H, t, *J* = 5.1 Hz, H-9) display the *α*-protons. The chemical shifts at δ_H 2.99, (dd, 14.2, 5.2 Hz) and δ_H 2.93 (dd, *J* = 14.2, 4.6 Hz) which display H-10, and aromatic doublets at δ_H 6.95 (2H, d, *J* = 8.1 Hz, H-3' and 5') and δ_H 6.60 (2H, d, *J* = 8.1 Hz, H-2' and 6'), indicating a para-substituted phenol. The ^{13}C NMR spectrum exhibited 14 carbons consist of amide carbonyls at δ_C 165.6 (C-1) and δ_C 169.8 (C-7), proline ring carbons at δ_C 44.6 (C-3, CH_2), δ_C 21.3 (C-4, CH_2), δ_C 27.9 (C-5, CH_2), and δ_C 58.6 (C-6, CH), tyrosine *α*-carbon at δ_C 56.4 (C-9, CH), *β*-carbon at δ_C 36.2 (C-10, CH_2), and aromatic carbons at δ_C 126.8 (C-1'), δ_C 130.7 (C-2' and C-6'), δ_C 114.6 (C-3' and C-5'), and δ_C 156.4 (C-4', phenolic C-OH).

COSY correlations linked the proline ring protons, H-3 to H-6 (Fig. 3), and the tyrosine methylene H-10 to H-9. HMBC cross-peaks from *α*-protons at H-6 and H-9 to C-7 and C-1, respectively, confirmed the DKP core. Additional HMBC from H-10 to aromatic carbons C-1', C-2' and C-6' verified the tyrosine attachment. The phenolic OH was inferred from the downfield C-4' signal and lack of a corresponding proton. The structure was assigned as cyclo(L-prolyl-L-tyrosyl), consistent with literature (Sunaryanto et al., 2011, Noël et al., 2017).

Compound **6** is structurally a hydroxylated analogue of **4**, the hydroxylated proline exhibited δ_C 67.1 for C-4, and reveled δ_H 4.17 for H-4. This proton showed COSY correlation to H-3 and H-5, HMBC cross peaks to C-3 and C-6, which confirmed hydroxyl group position at C-4 in proline moiety. The structure was assigned as cyclo(4-hydroxy-L-Pro-L-Phe), which were in consistent with the previous report on isolation of **6** from *S.coelicolor* LY001 purified from the sponge *Callyspongia siphonella* (Shaala et al., 2020).

3.7 LC-MS of DCM fraction of strains AHL19

The analysis of LC/MS chromatogram of the DCM extract of *S. canescens* AHL19, indicated the profile of isolated 2,5-DKPs. The total ion chromatogram (TIC) in positive and negative modes displayed multiple peaks, with the early elution of corresponding polar and small dipeptide, 2,5-DKPs, from about 1 to 10 minutes and later peaks indicative of larger polyketides or hydrophobic analogs. Molecular ions and adducts of 2,5-DKPs confirmed by matching *m/z* values in both ionization modes.

3.8 Molecular docking

The structures used in this study were DNA gyrase A (PDB ID: 5IWI), DNA gyrase B (PDB ID: 3U2D), DHFR (PDB ID: 3SRW), and *β*-tubulin (PDB ID: 5C8Y). Molecular docking calculations were used to assess the chemical activity of the compounds in the extracts that were presented when they interacted with the chosen enzymes. The results demonstrated the compounds' propensity for binding to the targets as well as the likely protein residues that may interact with the compounds. Table 4 displays the outcomes of the docking scores. The molecule **5** with the highest binding affinity, showed the lowest docking score against DHFR and *β*-tubulin, with a docking score of -8.108 and − 9.599 kcal/mol, respectively. Figure 4

shows the molecule **5** and streptomycin docking position and created interactions in the DHFR and *β*-tubulin binding sites.

For the DHFR protein, all tested DKPs formed hydrogen bonds except for compound **4**, which instead showed a π–π stacking interaction. Compounds **1**, **2**, **3**, and **5** interact via their carbonyl group as a hydrogen bond acceptor, while compound **6** interacts through its OH group at the C-4 position, which acts as a hydrogen bond donor. Notably, compound **5** forms an additional hydrogen bond through the OH group on its phenyl ring, engaging the Thr122 residue. It is evident that molecule **5** has formed two hydrogen bonds with DHFR's Ala8 and Thr122 residues. Streptomycin has a salt bridge interaction with Asp28 and two hydrogen bonds with Gln20 and Thr47 of DHFR.

For the *β*-tubulin protein, all tested DKPs formed hydrogen bonds. Compounds **2**, **3**, and **4** interact through the same two residues, Glu198 and Val236, acting as hydrogen bond acceptor and donor respectively, while compounds **1** and **6** with the lowest affinities form a single hydrogen bond with Leu253. Consistent with its behavior against DHFR, compound **5** forms an additional hydrogen bond through the OH group on its phenyl ring, engaging the Gln134 residue, beyond the Glu198 and Val236 interactions shared with compounds **2**, **3**, and **4**. There are three hydrogen bonds between molecule **5** and the residues Gln134, Glh198, and Val236 of *β*-tubulin.

In a 2023 study, the effect of hydroxyl groups on the anti-quorum-sensing and anti-biofilm activity of structurally similar cyclic dipeptides was investigated against *Pseudomonas aeruginosa* PAO1. The authors docked cyclo(L-Pro-L-Phe), cyclo(L-Hyp-L-Tyr), and cyclo(L-Pro-L-Tyr) against the quorum-sensing receptor LasR and found that the two Tyr-containing dipeptides, whose phenyl-ring's OH group formed a hydrogen bond, showed binding efficiencies similar to that of the natural autoinducer ligand 3OC12-HSL, whereas cyclo(L-Pro-L-Phe) exhibited lower affinity. These findings were further supported experimentally, consistent with the docking results (Li et al., 2023). These data are also consistent with our findings.

The docking scores for DNA gyrase A and B were not significant, therefore, these two targets cannot be considered viable targets of our compounds, owing to their very low binding affinities.

Based on our results, we conclude that, as with DHFR, the hydroxyl group on the phenyl moiety plays a critical role in lowering the binding energy and, consequently, improving the docking score, with compound **5** showing the highest binding affinity among all tested DKPs against β-tubulin. For a better comparison between the purified compounds, the 2D interactions of the isolates against DHFR and *β*-tubulin are presented in Figures S31-S42.

Table 4
Docking scores of 2,5-DKPs against DNA gyrase A, B, DHFR enzymes, and the cancer related target *β*-tubulin.

Target enzyme	Compound	Docking score	Target residues and interactions
DHFR	Compound **5**	-8.108	Ala8: H-bond, Thr122: H-bond
	Compound **4**	-6.591	Phe93: Pi-Pi stacking
	Compound **3**	-6.573	Ala8: H-bond
	Compound **6**	-6.514	Ala8: H-bond
	Compound **2**	-6.442	Thr122: H-bond
	Compound **1**	-6.055	Ala8: H-bond, Thr122: H-bond
	Streptomycin	-5.954	Gln20: H-bond, Thr47: H-bond, Asp28: Salt bridge
DNA Gyrase A	Compound **6**	-4.896	
	Compound **5**	-4.427	
	Compound **4**	-3.956	
	Compound **3**	-3.922	
	Compound **2**	-3.723	
	Compound **1**	-3.304	
	Streptomycin	-5.607	Glu88: H-bond, Ala118: H-bond, Asp437: Salt bridge
DNA Gyrase B	Compound **5**	-4.368	Arg84: Pi cation, Arg144: H-bond
	Compound **6**	-4.123	Arg84: H-bond, Arg144: H-bond, Gly85: H-bond
	Compound **4**	-3.979	-
	Compound **3**	-3.796	Arg144: H-bond, Gly85: H-bond
	Compound **2**	-3.625	Arg84: Pi cation, Arg144: H-bond
	Compound **1**	-3.342	Arg144: H-bond
	Streptomycin	-5.770	Glu58: H-bond, Glu58: Salt bridge, Arg144: H-bond
Tubulin B	Compound **5**	-9.599	Gln134: H-bond, Glh198: H-bond, Val236: H-bond
	Compound **4**	-9.358	Glh198: H-bond, Val236: H-bond
	Compound **2**	-8.420	Glh198: H-bond, Val236: H-bond
	Compound **3**	-8.415	Glh198: H-bond, Val236: H-bond

Target enzyme	Compound	Docking score	Target residues and interactions
	Compound **6**	-6.969	Leu2653: H-bond
	Compound **1**	-6.645	Leu2653: H-bond

3.9 MD simulation

The MD simulation for 100 ns was used to further assess the interactions of DHFR with molecule **5** and streptomycin, and compound **5** with *β*-tubulin. In these simulations, the protein's RMSD values converge at roughly 1.5 Å for the **5**-DHFR complex and 3 Å for the streptomycin-DHFR complex, respectively (Fig. 5). The RMSD fluctuations for *β*-tubulin have converged at about 1.8 Å. For the DHFR protein, this shows that the system stabilizes after 100 ns and that the protein fluctuates less when interacting with compound **5** than it does with streptomycin. As a result, compound **5** renders the protein more stable. The same trend is observed for the β-tubulin protein. Figure 6 displays the ligand-protein interactions between streptomycin-DHFR, **5**-DHFR, and **5**-β-tubulin following the simulation period. The residues Ala8, Gln96, Ile15, Thr122, and Asn15 have the largest interaction percentages with molecule **5**. During the simulation, the main interactions formed by Ala8, Gln96, and Thr122 are hydrogen bonds, while the main interaction for Ile15 is hydrophobic contact. Streptomycin primarily targets the residues Ser50, Leu21, Asn27, Leu25, and Trp23. With these residues, streptomycin has formed hydrophobic contacts, water bridge interactions, and hydrogen bonds. The residues that exhibited the highest interaction fraction in *β*-tubulin are Asn165, Val236, and Cys239. The formed interactions between these residues and compound **5** are both hydrogen bonds and water bridges. Figure 6 shows the specifics of further interactions between DHFR/ *β*-tubulin and these chemicals across a 100 ns simulation.

4. Conclusion

This research is the first report of isolation and characterization of six proline-based 2,5-diketopiperazines including cyclo (L-Pro-L-Val) (**1**), cyclo (L-Pro-L-Ile) (**2**), cyclo (L-Pro-L-Leu) (**3**), cyclo (L-Pro-L-Phe) (**4**), cyclo (L-Pro-L-Tyr) (**5**), and cyclo (4-hydroxy-L-Pro-L-Phe) (**6**) from the marine sponge *H. caerulea* symbionts bacterium, *S. canescens*. The ethyl acetate extract of the fermentation broth of *S. canescens* demonstrated strong antibacterial activity against *Staphylococcus aureus* and *Micrococcus luteus*, both with MIC values of 64 µg/mL, and against *Escherichia coli* with an MIC value of 128 µg/mL. These findings are consistent with the molecular docking results of the 2,5-DKPs isolated from this bioactive extract against the bacterial DHFR enzyme. Among the tested molecules, compound **5** showed selective and potent inhibition of DHFR, surpassing the binding affinity of streptomycin, an enzyme that plays a key role in bacterial proliferation. Compound **5** also exhibited strong binding affinity against cancer-related target *β*-tubulin, which shows that **5** can be considered a potent anticancer natural compound. Both the aqueous methanol and DCM fractions exhibited cytotoxicity against HT29 cells, and based on their chemical profiles, the DCM fraction was selected for further chromatographic isolation. The purification of these six DKPs from the most bioactive fraction along with previous studies, which

showed the antibacterial and cytotoxic activities of DKPs, emphasizing the therapeutic potential of these rigid, bioavailable cyclic dipeptides in addressing antibiotic resistance and cancer. These findings highlight the potential of marine microbial ecosystems as sustainable sources of novel bioactive compounds and pave the way for further investigations into their mechanisms, semisynthesis, and clinical applications to unlock new treatments for infectious and neoplastic diseases.

Declarations

Supporting Information

TLC, HPLC, and LC/MS chromatograms, along with spectral data including ^{1}H and ^{13}C NMR, ^{1}H-^{1}H COSY, HETCOR, and HMBC spectra, as well as 2D interaction data of compounds **1**-**6** with DHFR and β-tubulin are available as Supporting Information. Supplementary data related to this article can be found in the online version.

Declarations of competing interests

On behalf of all authors, the corresponding author states that there is no conflict of interest.

Author contributions: CRediT

ARJ: Supervision, Writing – review and editing, Project administration, Investigation, Funding acquisition, Data curation, Conceptualization. **SZ:** Writing – original draft, Methodology, Investigation, Formal analysis, Data curation, Conceptualization, **MG:** Writing – original draft, Methodology, Investigation, Formal analysis, Data curation, Conceptualization. **MA:** Methodology, Investigation, Data curation, Conceptualization. **OF:** Conceptualization, Data curation, Formal analysis, Writing – review & editing. **AP**: Conceptualization, Data curation, Formal analysis, Methodology, Writing – review & editing. **HES:** Formal analysis, Methodology, Writing – review & editing. All authors have read and approved the final manuscript.

Acknowledgements

The authors wish to acknowledge the National Institute for Medical Research Development of Iran (NIMAD, grant number: 964762) for the financial supports.

References

1. Alborz M, Gozari M, Firuzi O, Poustforoosh A, El Seedi HR, Jassbi AR (2025) Bioassay-Guided Purification of Cytotoxic Isoflavonoids and Sesquiterpenoids of Streptomyces coelicolor Isolated from Marine Sponge Axinella sinoxea, and In Silico Target Prediction. *Iran J Biotechnol*, 23: e4026. 10.30498/ijb.2025.489340.4026
2. Ansarizadeh A, Kafilzadeh F, Tamadoni Jahromi S, Kargar M, Gozari M (2023) Isolation, identification and evaluation of the anti-diabetic activity of secondary metabolites extracted from bacteria

associated with the Persian Gulf sponges (Haliclona sp. and Niphates sp). Iran J Fisheries Sci 22:511–525. 10.22092/ijfs.2023.129224

3. Arai M, Ishida S, Setiawan A, Kobayashi M (2009) Haliclonacyclamines, tetracyclic alkylpiperidine alkaloids, as anti-dormant mycobacterial substances from a marine sponge of Haliclona sp. Chem Pharm Bull (Tokyo) 57:1136–1138. 10.1248/cpb.57.1136
4. Bailly C (2025) Insights into the Bioactivities and Mechanism of Action of the Microbial Diketopiperazine Cyclic Dipeptide Cyclo(L-leucyl-L-prolyl). Mar Drugs 23:397
5. Bojarska J, Mieczkowski A, Ziora ZM, Skwarczynski M, Toth I, Shalash AO, Parang K, El-Mowafi SA, Mohammed EH, Elnagdy S (2021) Cyclic dipeptides: The biological and structural landscape with special focus on the anti-cancer proline-based scaffold. Biomolecules 11:1515
6. Bojarska J, Remko M, Breza M, Madura I, Fruziński A, Wolf WM (2020) A Proline-Based Tectons and Supramolecular Synthons for Drug Design 2.0: A Case Study of ACEI. Pharmaceuticals (Basel) 13. 10.3390/ph13110338
7. Borthwick AD (2012) 2,5-Diketopiperazines: Synthesis, Reactions, Medicinal Chemistry, and Bioactive Natural Products. Chem Rev 112:3641–3716. 10.1021/cr200398y
8. Chen C, Ye Y, Wang R, Zhang Y, Wu C, Debnath SC, Ma Z, Wang J, Wu M (2018) Streptomyces nigra sp. nov. Is a Novel Actinobacterium Isolated From Mangrove Soil and Exerts a Potent Antitumor Activity in Vitro. Front Microbiol 9:1587. 10.3389/fmicb.2018.01587
9. Cuong P, Cúc N, Quyen V, Binh P, Kiem P, Nam N, Nguyen TD (2014) Antimicrobial Constituents from the Bacillus megaterium LC Isolated from Marine Sponge Haliclona oculata. Nat Prod Sci 20:202–205
10. De Rosa S, Mitova M, Tommonaro G (2003) Marine bacteria associated with sponge as source of cyclic peptides. Biomol Eng 20:311–316. https://doi.org/10.1016/S1389-0344(03)00038-8
11. El-Saghier AM, Abosella L, Hassan A, Elakesh EO, Bräse S, Abuo-Rahma GE-DA, Aziz HA (2025) Design, synthesis, and in silico studies of New norfloxacin analogues with broad spectrum antibacterial activity via topoisomerase II inhibition. Pharmaceuticals 18:545
12. Fizza C, Israr M, Khan M, Sarwar A, Aziz T, Cui C, Zhao L, Alhomrani M, Alsanie W, Alamri A, Al-Asmari F, Al-Joufi F (2025) Cyclodipeptides (CDPs), the enzymatic synthesis, and the potential functional properties to exhibit broad varieties of pharmacological properties—A comprehensive review. Ital J Food Sci 37:131–152. 10.15586/ijfs.v37i1.2829
13. Giessen TW, Marahiel MA (2015) Rational and combinatorial tailoring of bioactive cyclic dipeptides. Front Microbiol 6:785. 10.3389/fmicb.2015.00785
14. Gozari M, Bahador N, Jassbi AR, Mortazavi MS, Eftekhar E (2018) Antioxidant and cytotoxic activities of metabolites produced by a new marine Streptomyces sp. isolated from the sea cucumber Holothuria leucospilota. Iran J Fisheries Sci 17:413–426
15. Gozari M, Bahador N, Mortazavi MS, Eftekhar E, Jassbi AR (2019) An olivomycin A derivative from a sponge-associated Streptomyces sp. strain SP 85. *3 Biotech*, 9: 439. 10.1007/s13205-019-1964-5

16. He R, Wang B, Wakimoto T, Wang M, Zhu L, Abe I (2013) Cyclodipeptides from Metagenomic Library of a Japanese Marine Sponge. J Braz Chem Soc 24:1926–1932. 10.5935/0103-5053.20130240
17. Heuer H, Krsek M, Baker P, Smalla K, Wellington E (1997) Analysis of actinomycete communities by specific amplification of genes encoding 16S rRNA and gel-electrophoretic separation in denaturing gradients. Appl Environ Microbiol 63:3233–3241
18. Huang R-M, Yi X-X, Zhou Y, Su X, Peng Y, Gao C-H (2014) An Update on 2,5-Diketopiperazines from Marine Organisms. Mar Drugs 12:6213–6235
19. Huang R, Zhou X, Xu T, Yang X, Liu Y (2010) Diketopiperazines from Marine Organisms. Chem Biodivers 7:2809–2829. https://doi.org/10.1002/cbdv.200900211
20. Jorgensen JH, National Committee for Clinical Laboratory, Standards IB (1997) Methods for dilution antimicrobial susceptibility tests for bacteria that grow aerobically: approved standard. NCCLS, Wayne, PA
21. Jung D, Machida K, Nakao Y, Owen JS, He S, Kindaichi T, Ohashi A, Aoi Y (2022) Cultivation of previously uncultured sponge-associated bacteria using advanced cultivation techniques: A perspective on possible key mechanisms. Front Mar Sci 9–2022. 10.3389/fmars.2022.963277
22. Kawato N, Shinobu R (1959) On Streptomyces herbaricolor sp. nov. Supplement: simple technique microscopic observation Mem Osaka Univ Lib Arts Educ B Nat Sci 8:114–119
23. Kieser T, Bibb M, Buttner M, Chater K, Hopwood D (2000) Practical streptomyces genetics: John innes foundation. Norwich Res Park Colney : 44–61
24. Kim H, Hwang JY, Shin J, Oh KB (2019) Inhibitory Effects of Diketopiperazines from Marine-Derived Streptomyces puniceus on the Isocitrate Lyase of Candida albicans. Molecules 24. 10.3390/molecules24112111
25. Kim J-A, Choi S-S, Lim JK, Kim E-S (2025) Unlocking marine treasures: isolation and mining strategies of natural products from sponge-associated bacteria. Nat Prod Rep. 10.1039/D5NP00013K
26. Kupchan SM (1970) Recent advances in the chemistry of terpenoid tumor inhibitors. Pure Appl Chem 21:227–246. 10.1351/pac197021020227
27. Li L, Xu Z, Cao R, Li J, Wu CJ, Wang Y, Zhu H (2023) Effects of hydroxyl group in cyclo(Pro-Tyr)-like cyclic dipeptides on their anti-QS activity and self-assembly. iScience 26:107048. 10.1016/j.isci.2023.107048
28. Li X, Dobretsov S, Xu Y, Xiao X, Hung OS, Qian PY (2006) Antifouling diketopiperazines produced by a deep-sea bacterium, Streptomyces fungicidicus. Biofouling 22:201–208
29. Liang H-X, Guo W-Y, Yang Z-Y, Lian X-Y, Wang Z-C, Li D-C, Liao X-J, Chen G-D, Xu S-H, Zhao B-X (2025) Haliclomeroterpenes A–D: Four Meroterpenes with Unprecedented Skeletons from the Marine Sponge Haliclona sp. J Org Chem 90:6504–6510. 10.1021/acs.joc.5c00340
30. Liang J, She J, Fu J, Wang J, Ye Y, Yang B, Liu Y, Zhou X, Tao H (2023) Advances in Natural Products from the Marine-Sponge-Associated Microorganisms with Antimicrobial Activity in the Last Decade. Mar Drugs 21. 10.3390/md21040236

31. Mehbub MF, Yang Q, Cheng Y, Franco CMM, Zhang W (2024) Marine sponge-derived natural products: trends and opportunities for the decade of 2011–2020. Front Mar Sci 11–2024. 10.3389/fmars.2024.1462825
32. Nazemi M, Moradi Y, Rezvani GF, Ahmaditaba MA, Gozari M, Salari Z (2017) Antimicrobial activities of semi polar-nonpolar and polar secondary metabolites of sponge Dysidea pallescens from Hengam Island. Persian Gulf 16:200–209
33. Noël A, Ferron S, Rouaud I, Gouault N, Hurvois JP, Tomasi S (2017) Isolation and Structure Identification of Novel Brominated Diketopiperazines from Nocardia ignorata-A Lichen-Associated Actinobacterium. Molecules 22. 10.3390/molecules22030371
34. Obled AMC, Hamed RB, Spence E, Zacharova MK, Sharma SV, Wang Y, Lynch R, Connaris H, Tatheer A, Bourguet-Kondracki ML, Florence GJ, Goss RJM (2025) Isolation and Identification of Cis-2,5-Diketopiperazine from a Novel Bacillus Strain and Synthesis of Its Four Stereoisomers. Mar Drugs 23. 10.3390/md23060234
35. Otsuka Y, Arita H, Sakaji M, Yamamoto K, Kashiwagi T, Shimamura T, Ukeda H (2019) Investigation of the formation mechanism of proline-containing cyclic dipeptide from the linear peptide. Biosci Biotechnol Biochem 83:2355–2363
36. Panwar U, Singh SK (2021) Atom-based 3D-QSAR, molecular docking, DFT, and simulation studies of acylhydrazone, hydrazine, and diazene derivatives as IN-LEDGF/p75 inhibitors. Struct Chem 32:337–352
37. Pourmozaffar S, Tamadoni Jahromi S, Gozari M, Rameshi H, Gozari M, Pazir MK, Sarvi B, Abolfathi M, Nahavandi R (2023) The first reporting of prevalence Vibrio species and expression of HSP genes in rayed pearl oyster (Pinctada radiata) under thermal conditions. Fish Shellfish Immunol 139:108907. 10.1016/j.fsi.2023.108907
38. Poustforoosh A (2025) Scaffold Hopping Method for Design and Development of Potential Allosteric AKT Inhibitors. Mol Biotechnol 67:3960–3974. 10.1007/s12033-024-01307-2
39. Poustforoosh A (2026) Design and assessment of amino acid-based gemini catanionic niosomes for dual-drug delivery of anticancer drug combination: a comprehensive computational study. Sci Rep. 10.1038/s41598-026-60899-8
40. Poustforoosh A, Elyasi M Leveraging Scaffold Hopping and Machine Learning for the Innovative Design and Assessment of Pyridine Derivatives as c-Met Inhibitors Using Amide-based Bioisosteres. J Comput Biophys Chem, 0: 1–15. 10.1142/s2737416526500110
41. Poustforoosh A, Sepahi S, Elyasi M (2025) Innovative Design and Assessment of Dual-targeted c-Met/PARP1 Inhibitors Using Pyridine-2-amine Bioisosteres: Scaffold Hopping, Machine Learning, Molecular Docking, Molecular Dynamics, and ADME/T Analysis. Adv Theory Simulations 18:e01220
42. Sahiba N, Joshi D, Agarwal LK, Manhas A, Teli P, Agarwal S (2024) Screening of synthesized perimidine compounds for the assessment of antimicrobial potential: in-vitro and in-silico molecular docking and molecular dynamics simulation studies. Discover Chem 1:30

43. Saquib Q, Schwaiger S, Alilou M, Ahmed S, Siddiqui MA, Ahmad J, Faisal M, Abdel-Salam EM, Wahab R, Al-Rehaily AJ, Stuppner H, Al-Khedhairy AA (2023) Marine Natural Compound (Neviotin A) Displays Anticancer Efficacy by Triggering Transcriptomic Alterations and Cell Death in MCF-7 Cells. Molecules 28:6289
44. Shaala LA, Youssef DTA, Alzughaibi TA, Elhady SS (2020) Antimicrobial Chlorinated 3-Phenylpropanoic Acid Derivatives from the Red Sea Marine Actinomycete Streptomyces coelicolor LY001. Mar Drugs 18. 10.3390/md18090450
45. Shaala LA, Youssef DTA, Badr JM, Harakeh SM, Genta-Jouve G (2019) Bioactive Diketopiperazines and Nucleoside Derivatives from a Sponge-Derived Streptomyces Species. Mar Drugs 17:584
46. Shafiq Osw P, Kareem Samad M, Mohammed Ayoob M, Muhammad Hamasalih R, Noori Abdullah M, Emam Hawaiz F, Caprioglio D, Minassi A, Amin HIM (2024) Facile ring opening of novel bisoxazolone with substituted aromatic amines: synthesis, antimicrobial, antioxidant potential, in silico ADME profile and molecular docking study. ChemistrySelect 9:e202401963
47. Shirling ET, Gottlieb D (1966) Methods for characterization of Streptomyces species. Int J Syst Bacteriol 16:313–340
48. Sirin S, Pearlman DA, Sherman W (2014) Physics-based enzyme design: Predicting binding affinity and catalytic activity. Proteins Struct Funct Bioinform 82:3397–3409
49. Song Z, Hou Y, Yang Q, Li X, Wu S (2021) Structures and Biological Activities of Diketopiperazines from Marine Organisms: A Review. Mar Drugs 19:403
50. Sun S-J, Liu Y-C, Weng C-H, Sun S-W, Li F, Li H, Zhu H (2020) Cyclic Dipeptides Mediating Quorum Sensing and Their Biological Effects in Hypsizygus Marmoreus. Biomolecules 10:298
51. Sunaryanto R, Marwoto B, Hartoto L, Mas'ud ZA, Irawadi TT (2011) Cyclo (Tyrosyl-Prolyl) produced by Streptomyces sp.: bioactivity and molecular structure elucidation. Microbiol Indonesia 5:5–5
52. Tian Z, Chu Y, Wang H, Zhong L, Deng M, Li W (2018) Biological activity and interaction mechanism of the diketopiperazine derivatives as tubulin polymerization inhibitors. RSC Adv 8:1055–1064
53. Turkez H, Cacciatore I, Arslan ME, Fornasari E, Marinelli L, Di Stefano A, Mardinoglu A (2020) Histidyl-Proline Diketopiperazine Isomers as Multipotent Anti-Alzheimer Drug Candidates. *Biomolecules*, 10. 10.3390/biom10050737
54. Williams S (1989) Genus Streptomyces waksman and henrici 1943. Bergey's Man Syst Bacteriol 4:2452–2492
55. Ying J, Lin R, Xu P, Wu Y, Liu Y, Zhao Y (2018) Prebiotic formation of cyclic dipeptides under potentially early Earth conditions. Sci Rep 8:936. 10.1038/s41598-018-19335-9
56. Zare S, Mirkhani H, Firuzi O, Moheimanian N, Asadollahi M, Pirhadi S, Chandran JN, Schneider B, Jassbi AR (2020) Antidiabetic and cytotoxic polyhydroxylated oleanane and ursane type triterpenoids from Salvia grossheimii. Bioorg Chem 104:104297. https://doi.org/10.1016/j.bioorg.2020.104297
57. Zhang Z, Schwartz S, Wagner L, Miller W (2000) A greedy algorithm for aligning DNA sequences. J Comput Biol 7:203–214

58. Zhu J, Liu Y, Liu Z, Wang H, Zhang H (2019) Bioactive Nitrogenous Secondary Metabolites from the Marine Sponge Genus Haliclona. Mar Drugs 17. 10.3390/md17120682

Figures

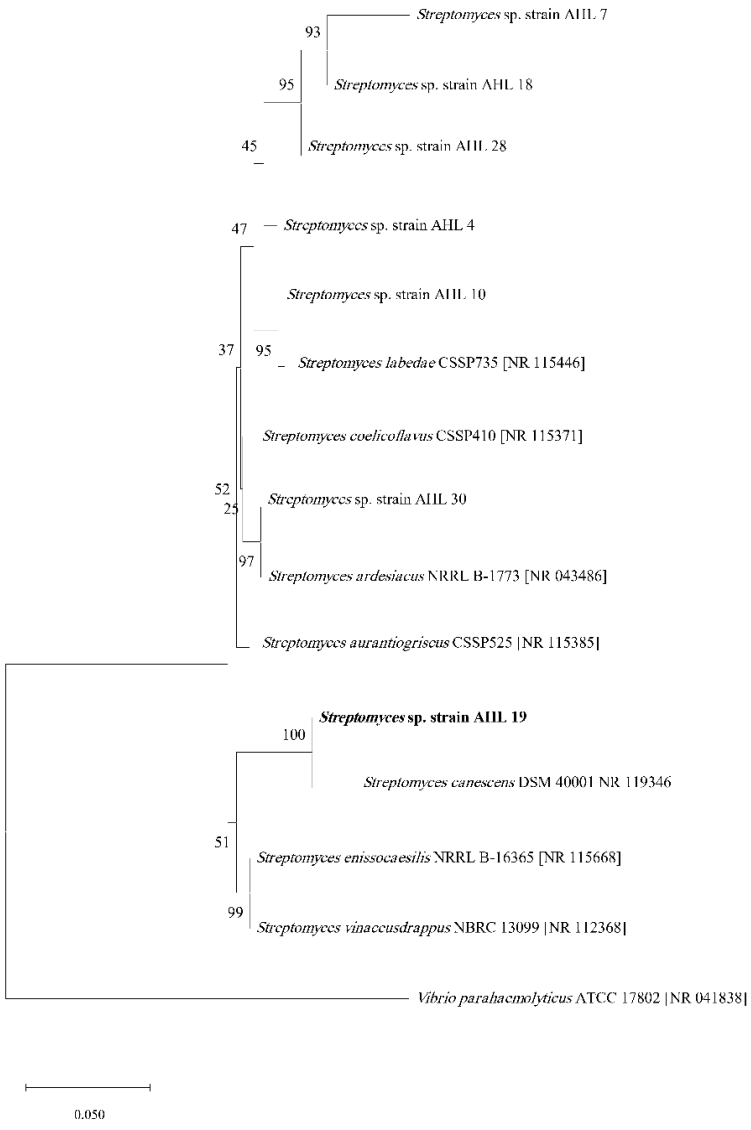


Figure 1

Phylogenetic dendrogram based on 16S rRNA gene analysis, reconstructed from evolutionary distances by using the neighbor-joining method, showing the phylogenetic position of potent strains and the closest related strains. *Vibrio parahaemolyticus* ATCC 17802 was used as an out-group. Bootstrap values are indicated at the relevant branching points. Numbers of branch node are bootstrap value based on 1000 resampling. Bar: 0.05 substitutions per nucleotide position

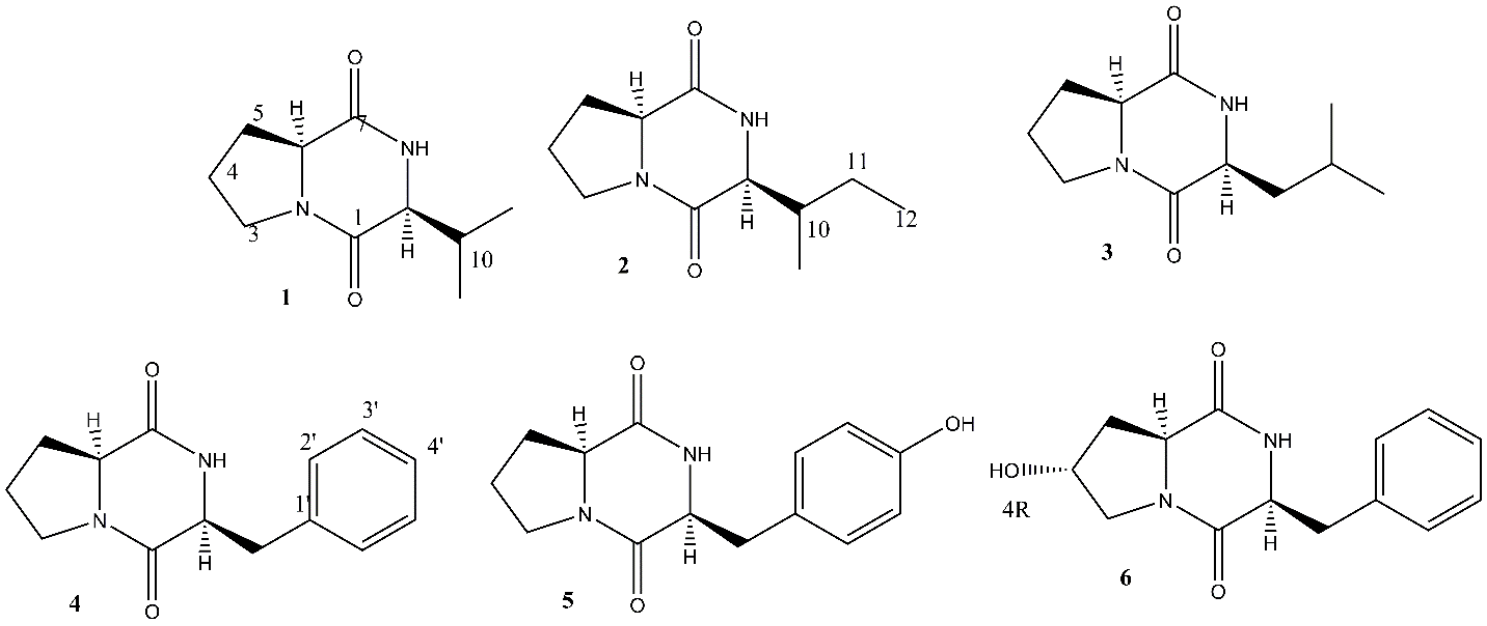


Figure 2

Chemical structures of 2,5-diketopiperazine cyclic dipeptides (**1**-**6**) from *Streptomyces canescens*

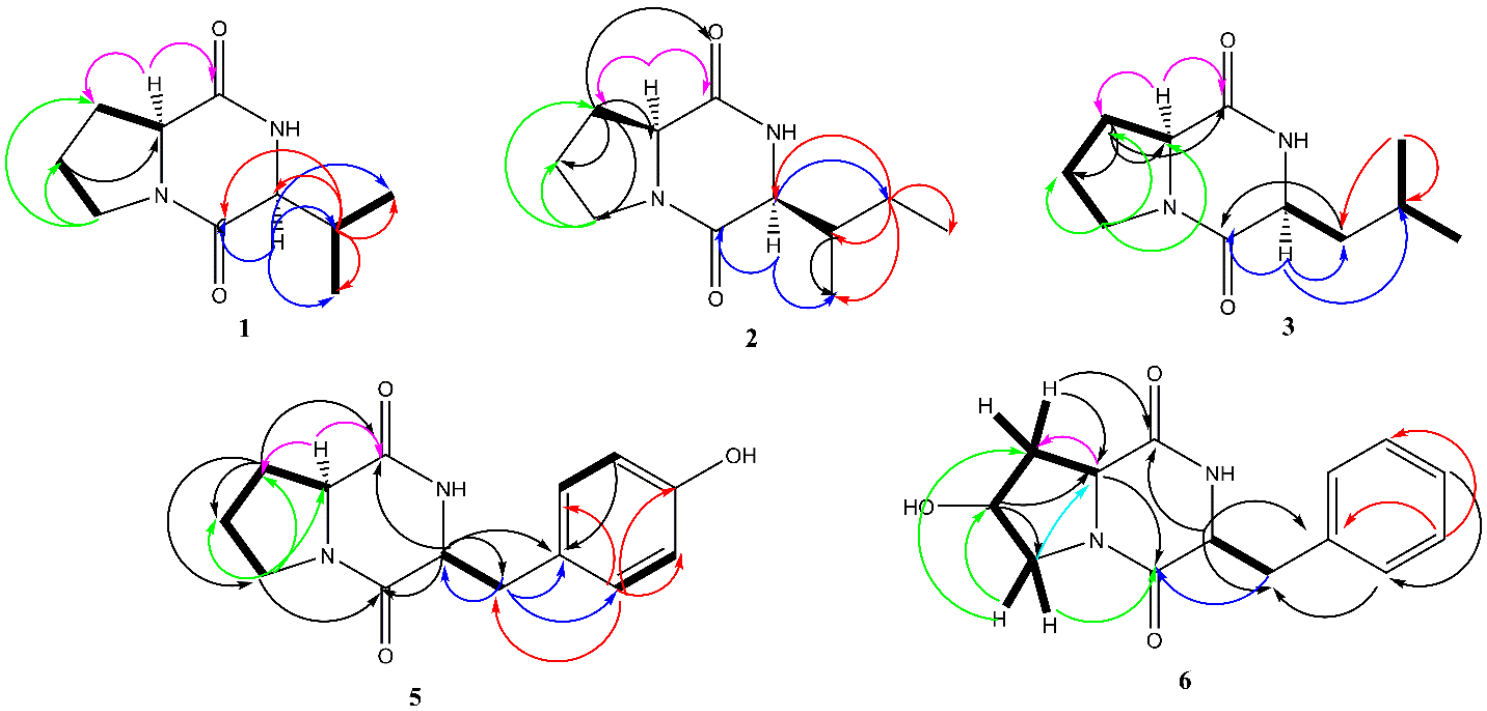


Figure 3

Key ^{1}H-^{1}H COSY and HMBC of 2,5-diketopiperazine cyclic dipeptides (**1-3**, **5**, **6**) from *Streptomyces canescens*

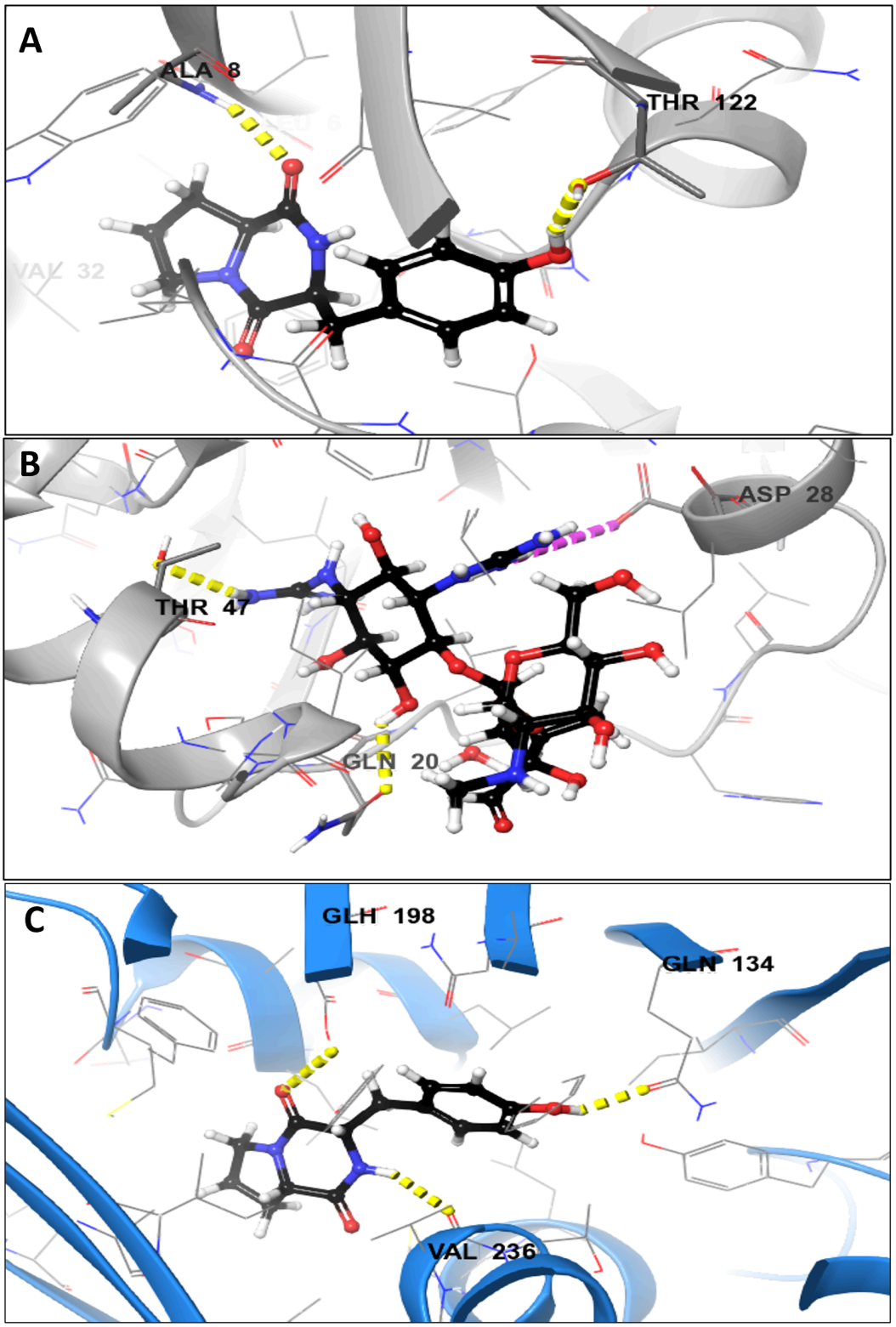


Figure 4

The docking pose and constructed interactions of **5** (A) and Streptomycin (B) in the active site of DHFR, and **5** in the active site of *β*-tubulin (C). The yellow and purple dashed lines indicate hydrogen bond and

salt bridge, respectively.

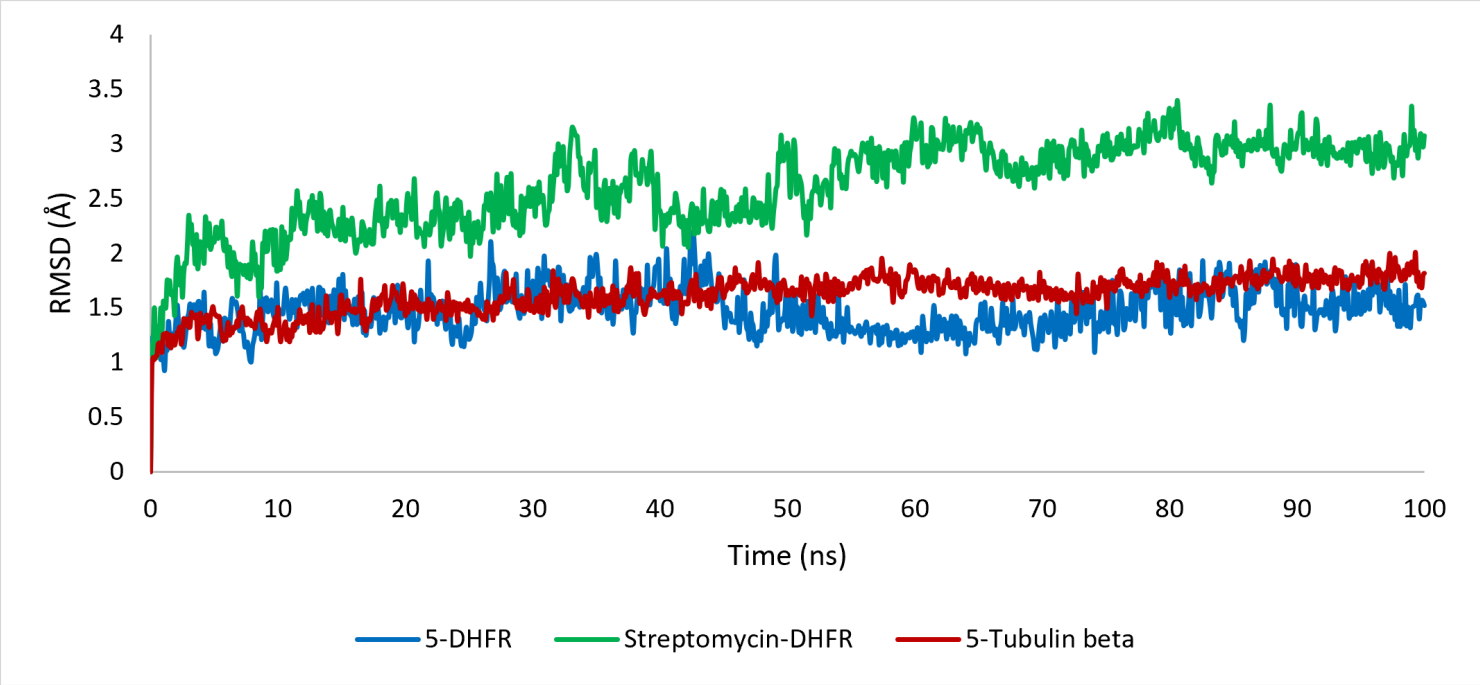


Figure 5

The RMSD values of DHFR when interacting with **5** (blue), Streptomycin (green), and *β*-tubulin (red). The protein structures are more stable when interacting with molecule **5** compared to streptomycin.

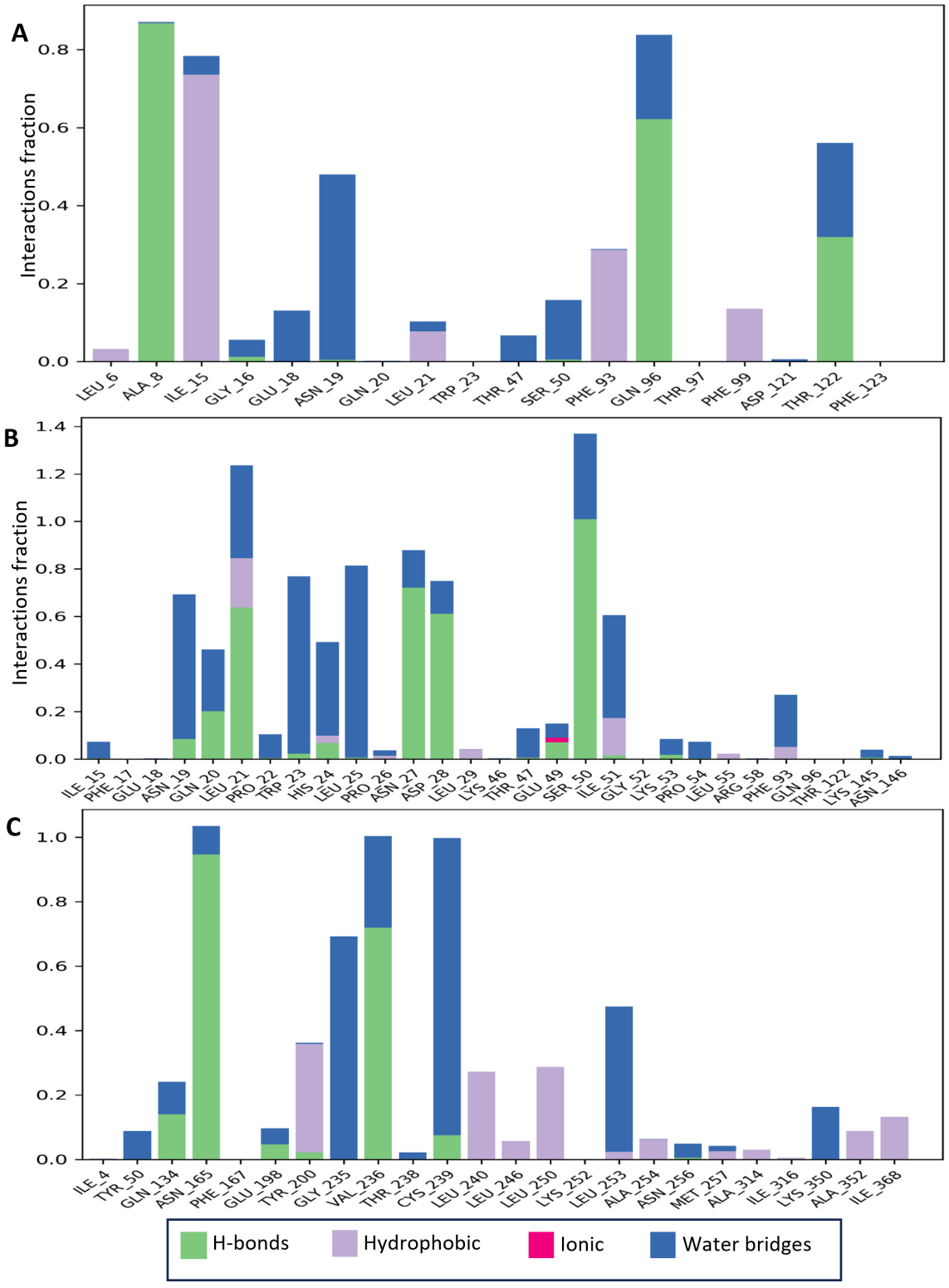


Figure 6

The interactions constructed between the compounds **5**-DHFR (A), Streptomycin-DHFR (B), and **5**-tubulin Beta (C) during the MD simulation.

Supplementary Files

This is a list of supplementary files associated with this preprint. Click to download.

- supplementarymaterial.docx